ACS APPLIED MATERIALS & INTERFACES

Research Article

www.acsami.org

Multiscaling Approach for Non-Destructive Adhesion Studies of Metal/Polymer Composites

Marieke Füllbrandt, Dikran Kesal, and Regine von Klitzing*

Technische Universität Berlin, Stranski-Laboratorium, Str. des 17.Juni 124, 10623 Berlin, Germany

Supporting Information

ABSTRACT: The adhesion of polyamide 6 (PA6) and polyethylene (PE) toward an aluminum alloy (Al-A) and a dual phase steel (DPS) is studied by contact angle (CA) measurements and atomic force microscopy (AFM). With the combination of the two methods the adhesion properties on a macro- and (sub)microscopic scale can be determined in a nondestructive way. The work of adhesion per area (W_{ad}) of the studied metal/polymer hybrids qualitatively scales the same on both length scales, that is, Al-A/PA6 > DPS/PA6 > Al-A/PE, DPS/PE. The polymer dominates the adhesion. The lower adhesion for PE toward the metal surfaces is explained by dominating van der Waals attraction forces, whereas adhesion for PA6 can also be attributed to attractive polar forces such as hydrogen bonding. For metal/PA6, W_{ad} on a macro- and microscopic length scale is similar. For metal/PE, a discrepancy is measured with lower adhesion values on the microscopic scale than on the macroscopic scale.

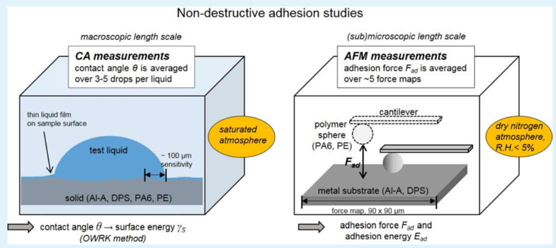

KEYWORDS: *adhesion, polymer/metal composites, atomic force microscopy, colloidal probe, roughness, rabinovich model, contact angle, surface energy*

1. INTRODUCTION

The adhesion between metals and polymeric materials plays a major role in many industrial fields, for example, in lightweight constructions used in the automotive, aircraft, and aerospace industry where they combine a high functional integration with a lower weight compared to pure metal parts. Metal/polymer hybrids are also of high interest for food packaging and for biomedical and electronic applications. The joining of these dissimilar materials without using additional components such as adhesives or primers is a central challenge. A fundamental understanding about the adhesion mechanisms at the metal/polymer interface on different length scales is essential. Conventionally, the connection between metals and polymers (e.g., thermoplastics) is realized by adhesion bonding, screwed fastening or mold-in technique during injection molding.[1,2] However, a direct adhesion without using any additives is desired. Motivated by (1) the growing needs of the industry for better adhesion properties between polymer and metal components and (2) an improved economical joining process, the fundamental understanding of the adhesion mechanisms at the metal/polymer interface is a main research focus. In this context, especially the adhesion phenomena on a (sub)-microscopic scale are of interest to better understand and control adhesion in often complex industrial situations.

Various tests, including peel-test, lap shear test, torque test, scratch test and pull-off test,[3,4] exist to directly measure adhesion properties. However, most of these methods are not only destructive but also not suited to reveal adhesion information on a micro- or even nanoscopic level. In this study, a new nondestructive multiscale approach is used to investigate the adhesion behavior between metals and polymers using atomic force microscopy (AFM) and contact angle (CA) measurements. AFM has become an important method to measure adhesion forces on a (sub)micrometer scale in a direct way. Using the colloidal probe (CP) technique introduced in 1991 by Ducker et al.,[5] it is possible to detect adhesion forces between a probe and flat substrate on a micro- and nanoscopic length scale. The technique is well-established for studying the surface interactions and mechanical properties between all kinds of colloidal particles and surfaces, including not only the field of material science but also biological and pharmaceutical systems. A review about the technique and its application in adhesion measurements can be found in literature.[6] One of the most important parameters affecting adhesion is surface roughness, a common feature of technical surfaces. Roughness must be taken into account when interpreting experimentally measured AFM adhesion forces. Various studies can be found in literature dealing with the influence of surface roughness on measured adhesion forces by AFM.[7−18] A more detailed discussion addressing this issue is given in the theoretical part of this paper. The adhesion on a macroscopic scale was calculated from contact angle (CA) measurements using the Owens−Wendt−Rabel−Kaelble (OWRK) method.[19,20] Compared to AFM, CA measurements determine the work of adhesion per area between two solid components in an indirect

Received: March 5, 2015
Accepted: July 9, 2015
Published: July 9, 2015

DOI: 10.1021/acsami.5b01949
ACS Appl. Mater. Interfaces 2015, 7, 16247−16256

way. However, information such as a division of the surface energy into dispersive and polar components can be obtained.

Both methods, AFM and CA, are commonly used to determine adhesion properties of surfaces. However, in most cases, macroscopic adhesion values are used for the interpretation of the AFM results. Moreover, adhesion studies of technically relevant metal/polymer systems down to (sub)microscale lengths are rare in literature due to the high complexity of the materials including surface roughness features. The aim of this work is, on one hand, to determine the work of adhesion per area from AFM measurements independently from macroscopic values (CA measurements). The measured adhesion force F_{ad} is converted to a work of adhesion per area considering the effect of surface roughness. On the other hand, the relationship between macro- and microscopic adhesion properties for the different metal/polymer hybrids is discussed. A scheme of the measurement setup and statistics is presented in Figure 1.

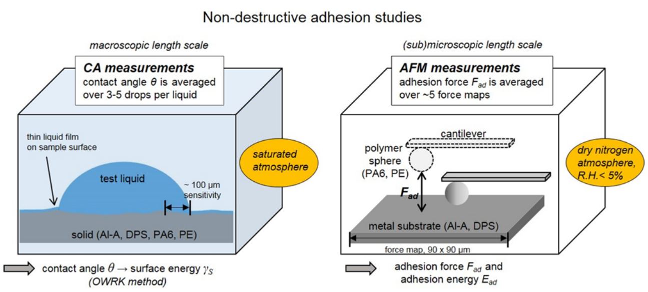

Figure 1. Schematic illustrations of measurement setups for (left) contact angle (CA) and (right) AFM force measurements.

Adhesion studies are performed for different metal/polymer pairs. The metal substrates are an aluminum alloy (Al-A) and a dual phase steel (DPS) sample. As polymer components, polyamide 6 (PA6) and polyethylene (PE), a polar and nonpolar thermoplastic, respectively, are chosen. This report begins with a Theory section discussing the analysis of force curves obtained from AFM measurements and the influence of surface roughness on measured adhesion forces. The Results section presents first macroscopic adhesion properties from CA measurements, followed by results from AFM force measurements describing the microscopic adhesion properties. The Discussion section deals first with the modeling of AFM results under the aspect of surface roughness. Second, measured AFM adhesion forces are related to a microscopic work of adhesion per area. Finally, the macro- and microscopic work of adhesion per area are correlated and commonalities, and discrepancies are discussed.

2. THEORY

2.1. Force−Distance Curve. Colloidal probe AFM is a technique for direct measurement of surface forces. It is a useful tool for studying surface interaction by means of force−distance curves. The basic concept is the measurement of forces between a tip or particle (microsphere) attached to the end of a cantilever and a sample surface. The technique is well described in literature[6,21−24] and not reviewed here.

A typical force−distance curve for a metal substrate and a PA6 microsphere is shown in Figure 2. The single steps are basically (1) the microsphere approach to the sample surface, (2) the jump-to-contact point, where the sphere is attracted

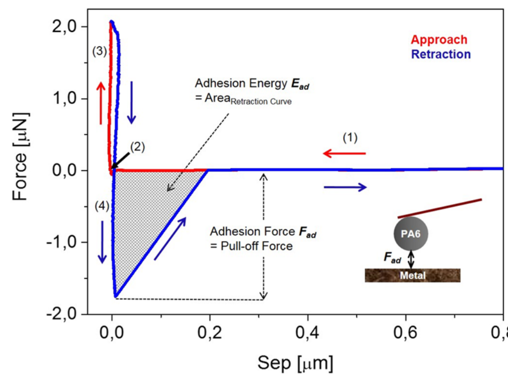

Figure 2. Typical experimental force−separation curve between a PA6 microsphere and a metal surface. Numbers 1−4 mark the single steps as described in the text.

toward the surface, followed by (3) sample indentation or compliance without deformation and cantilever deflection and (4) the retraction of the sphere, which might be hindered by adhesive forces (steps are indicated in Figure 2). The adhesion force (F_{ad}) between the colloidal probe and the sample is given by Hooke's law:

$$F_{ad} = -k_c \delta_{jump\text{-}off} \tag{1}$$

where k_c is the spring constant, and $\delta_{jump-off}$ is the jump-off-contact cantilever deflection. The adhesion energy (E_{ad}) can be obtained from the area under the retraction force−distance curve with the baseline taken at zero force (Figure 2).

2.2. Analysis of Adhesion Forces. Various adhesion models have been used to predict interactions between ideal surfaces based on (1) van der Waals adhesion (Hamaker approach)[25] or (2) through surface energy based approaches. For the latter, the adhesion forces (F_{ad}) can be related to a work of adhesion per area (W_{ad}) using contact mechanics models. Two contact models are often used: the Johnson−Kendall−Robert (JKR) model derived by Johnson et al.[26] in 1971 and the Derjaguin−Müller−Toporov (DMT) model derived by Derjaguin et al.[27] in 1975. Both are based on the Hertzian theory.[28] More detailed information can be found in literature.[21,24,29,30] The main difference between the two models lies in the assumed nature of forces acting between the particle and substrate. The JKR model assumes that attractive forces act only inside the particle-substrate contact area, whereas the DMT model includes long-range surface forces operating outside the particle-substrate contact area. For both models the correlation between F_{ad} and W_{ad} is described through a simple analytical equation as follows:

$$F_{ad} = c\pi R W_{ad} \tag{2}$$

where R is the radius of the microsphere attached to the cantilever, and c is a constant with $c = 2$ in the DMT and $c = 1.5$ in the JKR model.[7] The transition between these models can be predicted from a dimensionless parameter α suggested by Maugis[31] defined as

$$\alpha = \frac{2.06}{H_0}\sqrt[3]{\frac{RW_{ad}^2}{\pi K^2}} \tag{3}$$

where H_0 is the distance of closest approach between the contacting surfaces (≈0.3 nm), and K the reduced elastic modulus for the system under investigation.

DOI: 10.1021/acsami.5b01949
ACS Appl. Mater. Interfaces 2015, 7, 16247−16256

$$\frac{1}{K} = \frac{3}{4}\left(\frac{1-\nu_P^2}{E_P} + \frac{1-\nu_S^2}{E_S}\right) \tag{4}$$

ν and E refer to the Poisson's ratio and the elastic modulus, respectively, of the probe (P) and substrate (S). For $\alpha \geq 5$ the JKR model applies, whereas the DMT models applies for systems where $\alpha \leq 0.1$. For the transition region, the Maugis–Dugdale (MD) model[31] is the most appropriate.

2.3. Influence of Surface Roughness on Adhesion Forces. The JKR and DMT models assume a spherical particle in contact with a smooth surface (i.e., two ideal geometries). However, most materials have rough surfaces. Surface roughness at a micro- or nanoscale can significantly alter the true contact area between the colloidal probe and substrate from that predicted by the different contact mechanics models. That makes analysis of measured AFM pull-off forces challenging. In general, lower adhesion values than predicted from theory are obtained attributed mainly to surface roughness. Figure 3a illustrates the contact area for smooth surfaces as predicted by contact mechanics models (e.g., JKR and DMT). The variation in contact area due to roughness is demonstrated in Figure 3b,c: Asperities smaller than the microsphere (panel b) lead to a decrease in contact area whereas asperities comparable in size with the microsphere (panel c) can lead to an increase in the actual contact area. Figure 3b represents best the roughness scenario for the samples in this study. The size, shape, homogeneity, mechanical properties and distribution of the asperities influence the actual area of contact and directly affect the measured value of F_{ad}.[9]

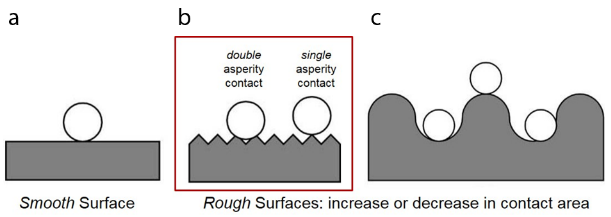

Figure 3. Scheme of contact scenarios for smooth and rough surfaces (not to scale) adapted from ref 9. (a) Contact areas for (a) smooth surface and rough surfaces with asperities (b) smaller than the particle size and (c) similar in size to the particles. The box marks the roughness scenario for the samples in this study.

A model to estimate adhesion forces for nanoscale rough surfaces has been described by Rumpf.[32] It is a Hamaker based approach taking only van der Waals forces acting between the surfaces into account. Based on the Rumpf model a modified and extended model has been proposed by Rabinovich et al.[33,34] The aim is to model the surface roughness in a way that describes the surface geometry of the substrate more precisely. The Rabinovich model takes into account the root-mean-square (rms) roughness parameters along with asperity sizes and distribution for a more realistic prediction of the adhesion forces. In addition, Rabinovich et al. noticed that many surfaces exhibit two scales of roughness (illustrated in Figure 4), rms_1 is associated with a longer peak-to-peak distance, λ_1, and rms_2 is associated with a shorter peak-to-peak distance, λ_2. The surface characteristics rms_1, rms_2, λ_1, and λ_2 can be obtained from AFM topography images. The total van der Waals adhesion force according to the Rabinovich model is given by eq 5 (for details, see ref 34):

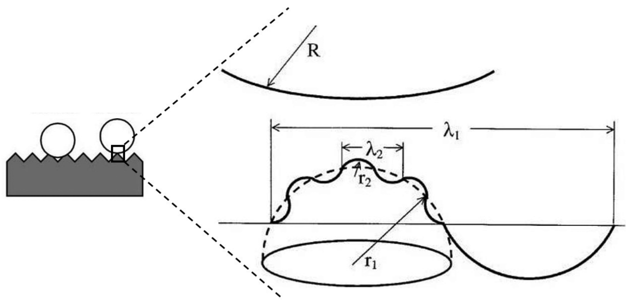

Figure 4. Geometry for surfaces with two types of roughness profiles according to the Rabinovich approach. Adapted from ref 34.

$$F_{ad} = \frac{AR}{6H_0^2}\left[\frac{1}{\left(1 + \frac{58R(\text{rms}_2)}{\lambda_2^2}\right)} + \frac{1}{\left(1 + \frac{58R(\text{rms}_1)}{\lambda_1^2}\right)\left(1 + \frac{1.82(\text{rms}_2)}{H_0}\right)^2}\right] \tag{5}$$

where A is the Hamaker constant. The first term in eq 5 accounts for contact interactions between the sphere and the asperities of the surface, whereas the second term describes noncontact interactions between the sphere and the substrate below the asperities.

A validation of the Rabinovich model for predicting adhesion forces between alumina substrates with defined nanoscale roughness is given by Laitinen et al.[35] They showed that the estimated adhesion forces using the Rabinovich model correspond well to experimental data even for technical rough surfaces. Kumar et al.[11] investigated adhesion forces between silica microspheres and different rough surfaces. Data could be well described by the Rabinovich approach.

If only one roughness scale is detectable or relevant, as in the present study (see Figure 14), then eq 5 reduces to

$$F_{ad} = \frac{AR}{6H_0^2}\left[\frac{1}{\left(1 + \frac{58R(\text{rms}_2)}{\lambda_2^2}\right)} + \frac{1}{\left(1 + \frac{1.82(\text{rms}_2)}{H_0}\right)^2}\right] \tag{6}$$

Eq 6 predicts adhesive interactions based only on attractive van der Waals forces. Other forces such as polar forces are not considered. However, polar forces, primarily hydrogen bonding, can play an important role in the adhesion behavior and might be equal or higher than the van der Waals contribution. The Rabinovich model can be extended to other adhesion models. Replacing the first term (contact interactions) of eq 6 by the adhesion force between two spheres as determined from the JKR or DMT theory leads to the following equation:

$$F_{ad} = \frac{c\pi W_{ad} R r_2}{r_2 + R} + \frac{AR}{6H_0^2}\frac{1}{\left(1 + \frac{1.82(\text{rms}_2)}{H_0}\right)^2} \tag{7}$$

The radius of asperity, r_2, can be replaced by[34]

$$r_2 = \frac{\lambda_2^2}{58\text{rms}_2} \tag{8}$$

DOI: 10.1021/acsami.5b01949
ACS Appl. Mater. Interfaces 2015, 7, 16247−16256

Even with more complex models considering surface energy and elastic deformation, the precision of the predicted adhesion properties is primarily dependent on how well roughness properties are characterized and resemble the true geometry of the surfaces.

3. RESULTS

3.1. Macroscopic Adhesion Properties Obtained from CA Measurements.

Table 1 lists the surface energies γ_S of the different polymer and metal samples. γ_S was determined using the OWRK method as described in the Experimental Section. The results agree well with surface energies found in literature for the respective materials.[36−39] Note that metals in general have high surface energies, whereas polymers have low surface energies. However, a native oxide layer and organic contamination on the metal surface reduce the surface energy of metals.[37] Here, the total surface energy of the metal and polymer samples is of the same magnitude. The metal samples show higher polar contributions than the polymer samples, especially the Al-A sample. As expected, the surface energy of the PE sample is mainly composed of a dispersive (i.e., nonpolar) contribution.

Table 1. Total Surface Energy Per Area (γ_S) with Dispersive and Polar Part of Polymer and Metal Samples As Determined from CA Measurements Using the OWKR Method

sample	total surface energy per area, γ_S (mN/m)	dispersive part, γ_S^d (mN/m)	polar part, γ_S^p (mN/m)
metal			
Al-A	48.3 ± 2.3	30.7 ± 2.0	17.6 ± 0.3
DPS	40.9 ± 3.3	31.2 ± 1.2	9.8 ± 2.1
polymer			
PA6	42.5 ± 3.1	37.0 ± 0.7	5.5 ± 2.4
PE	38.3 ± 2.0	36.5 ± 0.4	1.8 ± 1.5

The interfacial energy between a metal and polymer is calculated using eq 13 and subsequently inserted in eq 12 to obtain the macroscopic work of adhesion per area $W_{ad,CA}$. Results are given in Table 2. The macroscopic adhesion properties of the four metal/polymer combinations are in the same order of magnitude and only slight tendencies are observed: (1) both polymers show a slightly higher adhesion to Al-A than to the DPS sample, and (2) PA6 shows a higher adhesion to both metal samples compared to PE.

Table 2. Macroscopic Work of Adhesion Per Area from CA Measurements, $W_{ad,CA}$, for Different Metal/Polymer Pairs

sample pair (metal/polymer)	work of adhesion per area, $W_{ad,CA}$ (mN/m)
Al-A/PA6	87.1 ± 7.4
DPS/PA6	82.6 ± 6.7
Al-A/PE	78.2 ± 7.9
DPS/PE	75.9 ± 6.4

3.2. Microscopic Adhesion Properties Obtained from AFM Force Measurements.

3.2.1. Adhesion Force between PA6 and Metal Surfaces. The adhesion forces for Al-A/PA6 and DPS/PA6 are shown in Figure 5. Force data are plotted in a histogram and fitted with a Gaussian line. The corresponding mean adhesion force (F_{ad}), the standard deviation (σ), and the radius of the microsphere (R) are summarized in Table 3.

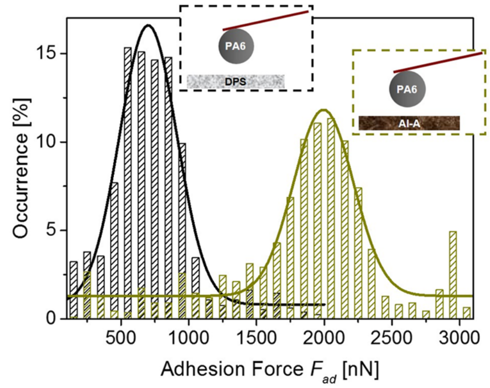

Figure 5. Adhesion force (F_{ad}) histogram obtained from AFM force mapping for (green) Al-A/PA6 and (black) DPS/PA6. The solid line is a Gaussian fit to the data.

Table 3. Results from AFM Force Measurements for Al-A/PA6 and DPS/PA6

parameter	Al-A/PA6	DPS/PA6
mean adhesion force, F_{ad} (nN)	1993.8	700.5
standard deviation, σ (nN)	221.4	211.6
radius of microsphere, R (μm)	12.9	7.9
normalized adhesion force, F_{ad}/R (N/m)	0.155	0.089

For a direct comparison of the force data, F_{ad} is normalized by the radius of the microsphere. The normalized adhesion force F_{ad}/R is also reported in Table 3 and indicates a stronger adhesion of PA6 to Al-A than to DPS. The trend was also supported from contact angle measurements (see Table 2). However, raw data from AFM force measurements have to be evaluated with care. To have more conclusive results, we discuss a detailed analysis considering roughness effects of sphere and substrate. Moreover, adhesion forces should be related to a work of adhesion per area (W_{ad}) in order to compare macro- and microscopic adhesion results.

3.2.2. Adhesion Force between PE and Metal Surfaces. Adhesion histograms for Al-A/PE and DPS/PE are shown in Figure 6. In contrast to PA6, PE is a nonpolar polymer. Therefore, the adhesion strength to metal surfaces is expected to be weaker.

On the basis of the normalized adhesion forces, one can state that indeed a lower adhesion force between the metal surfaces

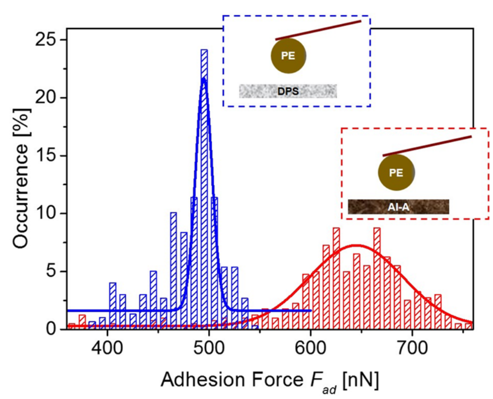

Figure 6. Adhesion force (F_{ad}) histogram obtained from AFM force mapping for (red) Al-A/PE and (blue) DPS/PE. The solid line is a Gaussian fit to the data.

DOI: 10.1021/acsami.5b01949
ACS Appl. Mater. Interfaces 2015, 7, 16247−16256

and PE is measured compared to the corresponding system with PA6. Results are summarized in Table 4. Moreover, the same trend than for the PA6 measurements is observed, that is, the normalized adhesion force between DPS/PE is slightly lower than between Al-A/PE. These findings are again in agreement with results from contact angle measurements (Table 2). However, as mentioned above, roughness features of sphere and substrate have to be considered allowing a more quantitative and qualitative analysis.

Table 4. Results from AFM Force Measurements for Al-A/PE and DPS/PE

parameter	Al-A/PE	DPS/PE
mean adhesion force, F_{ad} (nN)	645.7	494.1
standard deviation, σ (nN)	46.8	7.8
radius of microsphere, R (μm)	10.5	10.5
normalized adhesion force, F_{ad}/R (N/m)	0.061	0.047

3.2.3. Adhesion Energy. Besides the adhesion force, the adhesion energy E_{ad} can be extracted from force−distance curves. E_{ad} was evaluated from the area between approach and retraction curve (Figure 2) as done several times in literature.[40−44] It is correlated with the force as follows:[45]

$$E_{ad} = -\int_{x_2}^{x_1} F_{ad} dx \tag{9}$$

where F_{ad} is the pull-off or adhesion force, x is the probe-sample separation distance and $x_1 = 0$ and x_2 = jump-off position, the first and last point at which the curve crosses the zero force axis.

The adhesion energy histograms with the mean adhesion energy and its standard deviation are shown in Figure 7. Data are fitted to a Gaussian curve. At first glance, the adhesion energy does not scale with the corresponding adhesion force. Whereas the pair Al-A/PA6 shows the highest adhesion energy corresponding well with the highest adhesion force measured, all other pairs show the opposite trend. That means a decreasing adhesion energy with increasing adhesion force.

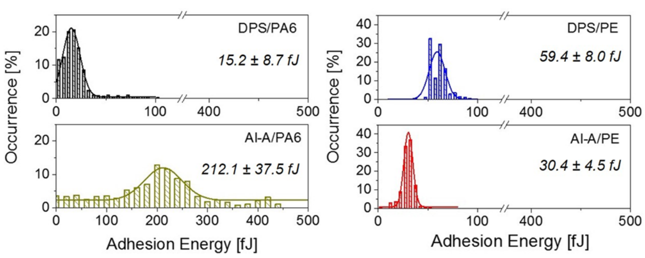

Figure 7. Adhesion energy E_{ad} histograms obtained from AFM force mapping for the different metal/polymer pairs. The solid line is a Gaussian fit to the data.

4. DISCUSSION

4.1. Modeling of AFM Force Data. Adhesion forces are strongly influenced by surface roughness because the true contact area between sphere and substrate alters with roughness. For a more quantitative and qualitative analysis of the measured adhesion forces, the surface roughness of the metal substrates and the polymeric microspheres has to be considered. Nanoscale asperities of polymeric microspheres can be deformed under an applied load. Such plastic deformations can be evaluated using a model proposed by Maugis and Pollock.[8,46] At a load of 1−2 μN, which is a typical load used in the described force measurements, asperities with a radius of curvature of maximum 20−30 nm for a PA6 and 80−120 nm for a PE microsphere should deform plastically. The surface irregularities on the polymeric microspheres are in the low nanometer range (as shown by SEM) and thus are most likely flattened during measurements. The roughness of the polymeric microspheres can thus be neglected in further calculations. However, the roughness of the metal substrates is of importance and has to be taken into account for the adhesion analysis. The influence of roughness on adhesion measurements is mainly visible in the tail of the adhesion force distribution[17,47] (see force histograms in the Results section).

Adhesion forces were calculated in the framework of the Rabinovich model using eq 6. The model suggests that the principal contribution to the adhesion force is van der Waals attraction. Figure 8 compares the normalized experimental and predicted adhesion forces. Data are plotted as a function of the variable rms_2. Values for Hamaker constants are taken from literature. The Hamaker constant, A_{11}, is approximately 7.9×10^{-20} J for PA6,[48] 8.43×10^{-20} J for PE,[49] 1.4×10^{-19} J for Al-A[45] and 2.1×10^{-19} J for DPS.[45] The Hamaker constant between two dissimilar materials, A_{12}, was estimated using a combining rule approximation:[45]

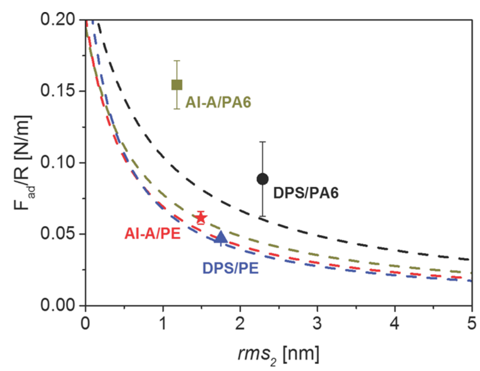

Figure 8. Experimental adhesion forces (symbols) and predicted values (dashed lines) in dependence on rms_2. Predictions are made using eq 6.

$$A_{12} = \sqrt{A_{11}A_{22}} \tag{10}$$

and resulted in $A_{12} = 1.05 \times 10^{-19}$ J for Al-A/PA6, $A_{12} = 1.29 \times 10^{-19}$ J for DPS/PA6, $A_{12} = 1.09 \times 10^{-19}$ J for Al-A/PE and $A_{12} = 1.33 \times 10^{-19}$ J for DPS/PE.

In general, a good agreement within order of magnitude in forces is achieved. Comparison of experimental and predicted data suggests that a large contribution to the adhesive behavior is van der Waals attraction. The experimental and predicted adhesion forces as well as their ratio are given in Table 5. Especially for the adhesion between metals and PE the model provides excellent predictions with a ratio of $F_{ad,experimental}/F_{ad,theoretical}$ close to one. PE is a nonpolar polymer without any functional groups. The adhesion to metal surfaces is therefore dominated by dispersion forces. For the metal/PA6 interactions a discrepancy exists. Adhesion forces are underestimated using the van der Waals based Rabinovich model. Especially for Al-A/PA6, the measured adhesion forces are larger than the theoretically predicted values by a factor of 2. This discrepancy can not only be explained by experimental error. As discussed in the theoretical part, other forces such as polar forces are not

DOI: 10.1021/acsami.5b01949
ACS Appl. Mater. Interfaces 2015, 7, 16247−16256

Table 5. Experimental and Predicted Adhesion Forces and Their Ratio[a]

sample pair (metal/polymer)	$F_{ad,experimental}$ [nN]	$F_{ad,theoretical}$ [nN]	$F_{ad,experimental}/F_{ad,theoretical}$
Al-A/PA6	1993.8	942.2	2.12
DPS/PA6	700.5	485.8	1.44
Al-A/PE	645.7	570.4	1.13
DPS/PE	494.1	478.4	1.03

[a]Predictions are made using eq 6.

considered in the proposed model. However, in contact interactions between metals and PA6 such forces may be important. Polar attractive forces arise probably from hydrogen bonding between the amide groups of PA6 and the hydroxyl groups of the metal surface.

4.2. Correlation between Macro- and Microscopic Adhesion. To compare the results of the macro- and microscopic adhesion experiments, we must convert AFM data into a work of adhesion per area. Two approaches to obtain a microscopic work of adhesion per area are discussed: (1) converting the adhesion force F_{ad} into a work of adhesion per area using contact mechanic models and (2) normalizing the adhesion energy E_{ad} by a contact area.

4.2.1. Relating F_{ad} to a Microscopic Work of Adhesion Per Area. A simple relation between F_{ad} and W_{ad} is given by the JRK and DMT model (see eq 2):

$$W_{ad} = \frac{F_{ad}}{c\pi R} \tag{11}$$

The approach requires the selection of an appropriate contact model for the interpretation of W_{ad}. Therefore, the dimensionless Maugis parameter α, which is a useful measure of which model is most appropriate, is estimated according to eq 3. Parameters used for the calculation are listed in Table 6.

Table 6. Elastic Modulus (E) and Poisson's Ratio (ν) for Metals and Polymers Used in This Study[a]

material	elastic modulus E (GPa)	Poisson's ratio (ν)
Al-A	69.0	0.33
DPS	200.0	0.30
PA6	2.0	0.39
PE	0.4	0.46

[a]Values are taken from data sheets (provided by suppliers) and ref 50.

For all metal/polymer pairs $\alpha \geq 5$ therefore the JKR model applies (with $c = 1.5$). Results for $W_{ad,JKR}$ are summarized in Table 7. Values are much smaller than expected, compared to results from CA measurements due to a wrong estimation of the contact area. As discussed above, AFM data should be analyzed using the Rabinovich model eq 7 to account for roughness effects of the metal substrates. Results for $W_{ad,Rabi}$ are given in Table 7. The comparison of $W_{ad,JKR}$ and $W_{ad,Rabi}$ shows that considering roughness effects leads to higher values for W_{ad} that are closer to values from contact angle measurements. An excellent correlation can be found for Al-A/PA6. For the other metal/polymer pairs AFM measurements yielded a lower work of adhesion per area compared to CA measurements, especially for the metal/PE combinations.

Table 7. Macroscopic and Microscopic Work of Adhesion Per Area

work of adhesion W_{ad} per area (mN/m) obtained from	Al-A/PA6	DPS/PA6	Al-A/PE	DPS/PE
CA measurements, $W_{ad,CA}$	87.1	82.6	78.2	75.9
JKR model, $W_{ad,JKR}$	32.8	18.8	13.0	9.9
Rabinovich model, $W_{ad,Rabi}$	89.2	73.5	48.7	54.1

Note that, while an excellent correlation for the work of adhesion per area from CA and AFM measurements were found for Al-A/PA6, experimental and predicted adhesion forces did not agree very well (compare Table 5). As discussed above, polar forces contributing to the adhesion force between Al-A and PA6 were not considered in the model used for predicting adhesion forces explaining the underestimation of the adhesion force using eq 6.

4.2.2. Relating E_{ad} to a Microscopic Work of Adhesion Per Area. A second approach is the evaluation of the adhesion energy E_{ad} from the area under the force curve upon retraction (see Figure 2).[40−44] That area corresponds to a work of adhesion. In order to obtain a work of adhesion per area, a normalization with the contact area is necessary. The contact area cannot be measured directly with the colloidal probe and must therefore be estimated. The estimation of the contact area for rough surfaces is not straightforward. In addition, the jump-out distances, and thus the area under the curve, depends on the cantilever stiffness. Because different cantilevers are used in this study, the comparison of the adhesion energy on a qualitatively level is not possible. For further discussions, this approach is not taken into account. A more detailed explanation and argumentation is given in the Supporting Information.

4.2.3. Comparison of Macro- And Microscopic Adhesion Results. For a further correlation of macro- and microscopic adhesion properties, the work of adhesion per area obtained from CA measurements $W_{ad,CA}$ and the Rabinovich model $W_{ad,Rabi}$ are used. Figure 9 shows the correlation between $W_{ad,CA}$ and $W_{ad,Rabi}$ for the different metal/polymer pairs. Between metals/PE the microscopically work of adhesion per area is remarkable smaller than the adhesion on a macroscopic scale. The values for metal/PA6 correlate well, an almost perfect correlation is obtained for Al-A/PA6. CA measurements resulted in similar values for the work of adhesion per area for all studied sample pairs. Values are in the range of 74.1−86.6 mN/m (Figure 9, gray box). Microscopic studies seemed to be more sensitive to the polymer component and revealed larger differences between metals/PA6 and metals/PE combinations with values between 48.7 and 89.2 mN/m (Figure 9,

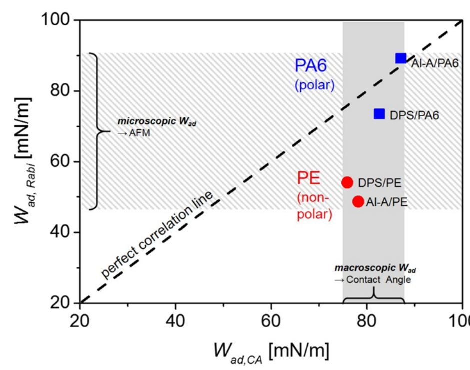

Figure 9. Correlation between macroscopic and microscopic work of adhesion per area for metal/polymer pairs.

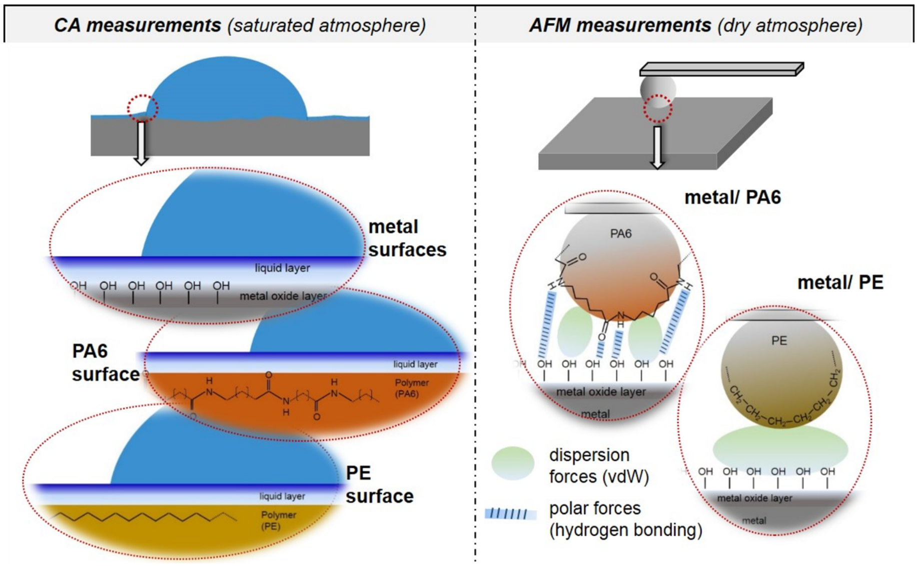

Figure 10. Scheme of interactions between metal and polymer surfaces measured by CA and AFM (not to scale).

shaded box). These differences in length scale adhesion properties might be explained as follows:

CA measurements are an indirect method to determine the work of adhesion per area. They are not conducted in a dry atmosphere; they are conducted in a saturated atmosphere using a test liquid. A thin liquid film might be present on all surfaces, reducing the sensitivity to (small) differences in surface composition and resulting in (1) similar surface energies for all measured surfaces and (2) consequently macroscopic adhesion properties that are in the same order of magnitude for all metal/polymer combinations, whereas AFM force measurements directly determine an adhesion force on a (sub)microscopic length scale taking local roughness features into account. Moreover, measurements are conducted in a dry nitrogen atmosphere, that is, at a RH < 5%, where capillary forces can be excluded. The higher sensitivity and the defined measurement parameters make it possible to probe pure interactions at the metal/polymer interface and to differentiate between different interactions. This results in different adhesion properties for metals/PA6 and metals/PE due to different chemical surface composition of the polymer. Interactions are sketched in Figure 10.

5. SUMMARY AND CONCLUSION

In the present investigations, the adhesion of polyamide 6 (PA6) and polyethylene (PE) toward an aluminum alloy (Al-A) and a dual phase steel (DPS) were studied by contact angle (CA) measurements and atomic force microscopy (AFM) measurements. Compared to standard adhesion tests, the combination of the two methods allowed to determine the adhesion properties on a macro- and (sub)microscopic scale in a nondestructive way. The surface energy of metal and polymer components, including the polar and dispersive parts, were obtained from CA measurements using the OWRK method. Values are further related to a macroscopic work of adhesion per area. Independent from the macroscopic values, a work of adhesion per area on a microscopic length scale was calculated from measured AFM adhesion forces. Roughness effects are considered using the Rabinovich model.

The work of adhesion per area of the studied metal/polymer systems scaled the same on both length scales. That was: Al-A/PA6 > DPS/PA6 > Al-A/PE, DPS/PE. The adhesion was found to be dominated by the polymer. The main results can be summarized as follows: (1) The lower adhesion for PE toward the metal surfaces is explained by dominating van der Waals attraction forces, whereas for PA6, attractive polar forces (e.g., hydrogen bonding forces), also contribute to the adhesion toward metals. (2) For the polar polymer PA6 and metal surfaces the macro- and microscopic work of adhesion per area resulted in a good agreement. For the nonpolar PE and metals a discrepancy was found with a lower work of adhesion per area on the micro- than macroscopic scale. (3) The undefined, saturated atmosphere in contact angle measurements led (a) to adhesion properties in the same order of magnitude for all metal/polymer combinations with only slight tendencies and (b) to a higher work of adhesion per area for the nonpolar PE/metal pairs compared to results from AFM measurements. (4) AFM measurements were conducted in a defined measurement atmosphere making it possible to distinguish better between polar and nonpolar interactions and, for example, exclude contributions from capillary forces.

The presented approach is useful to study the adhesion properties of technical metal/polymer hybrids in a non-destructive way on different length scales. The work of adhesion per area obtained from the two methods scaled the same for the different polymer/metal pairs and absolute values were in the same order of magnitude. However, with AFM force measurements it was possible to determine adhesion characteristics more precisely. In this way, different adhesion mechanisms depending on the chemical nature of the polymer could be identified.

6. EXPERIMENTAL SECTION

6.1. Materials. *6.1.1. Polymeric Microspheres and Substrates.* Thermoplastics are a common polymer class used for hybrid components. Two thermoplastics with different chemical properties were picked for the adhesion study, polyamide 6 (PA6) and polyethylene (PE). PA6 is a polar polymer with functional groups (amide group NH−CO), whereas PE is nonpolar without any functional groups on the backbone. The molecular structure of both polymers is shown in Figure 11.

For AFM measurements, polymeric microspheres made of PA6 (Phosphorex, Inc., Hopkinton, MA) and PE (Cospheric, Santa

DOI: 10.1021/acsami.5b01949
ACS Appl. Mater. Interfaces 2015, 7, 16247−16256

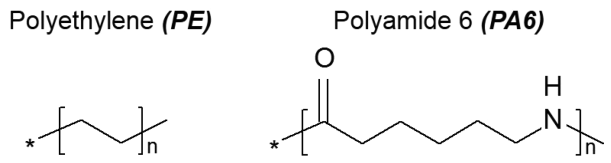

Figure 11. Molecular structure of polyethylene (PE) and polyamide 6 (PA6).

Barbara, CA) with a diameter of around 20 ± 7 μm are used. The microspheres are glued with epoxy to a tipless cantilever with a given spring constant of 5−17 N/m (NSC35 MikroMasch). The spring constant of the cantilever was determined using the thermal method, which is based on fitting a thermal spectrum (harmonic oscillator model) of the cantilever motion.[51] Before the thermal method was applied, the cantilever deflection (bending) was correlated to the z-piezo movement (optical lever sensitivity) by conducting a measurement on a hard surface. Microspheres were characterized by optical microscopy and scanning electron microscopy (SEM) in order to obtain information about size and surface roughness. SEM images of PA6 and PE microspheres attached to a cantilever are presented in Figure 12. The microspheres exhibit a spherical shape and a smooth surface. The surface of the PE spheres are slightly rougher than the surface of the PA6 spheres. Note that SEM imaging requires a carbon or gold coating of the sample due to charging effects and therefore can be only done after the experiments.

For CA measurements, injection molded PA6 and PE plates are used. Samples were kindly provided by NMF GmbH, Fürth (Germany).

6.1.2. Metal Substrates. An aluminum alloy ($AlMg_{4,5}Mn_{0,4}$) and a dual phase steel (DPS) commonly used in industrial applications were chosen as metal substrates for adhesion studies. They are referred to in the following as Al-A and DPS sample, respectively. Technical surfaces exhibit a quite rough surface (micrometer range) not suitable for AFM investigations. Therefore, Al-A and DPS samples were mechanically polished to obtain a rather smooth surface with a nanometer-scale roughness. A careful analysis of the surface roughness is necessary to evaluate the measured adhesion forces. That includes the determination of the root-mean square roughness (rms) and the peak-to-peak distance (λ).

Roughness characteristics of metal samples were obtained from AFM topography measurements. Imaging was performed with a MFP3D AFM instrument (Asylum Research, Santa Barbara, CA) in air and tapping mode at room temperature. Examples of a polished Al-A and DPS substrate are shown in Figure 13. The metal surfaces showed only one type of roughness profile described through rms_2 and the corresponding λ_2 (Figure 4). The roughness parameters and the asperity radius r_2 of the metal samples are given in Table 8. The root-mean-square roughness and the peak-to-peak distance were determined by using the analysis software of the AFM. The peak-to-peak distance was extracted from section graphs (Figure 14) taken in different directions over different distances. All values are average results from analysis done on different positions of the sample surface. The asperity radius r_2 is calculated using eq 8.

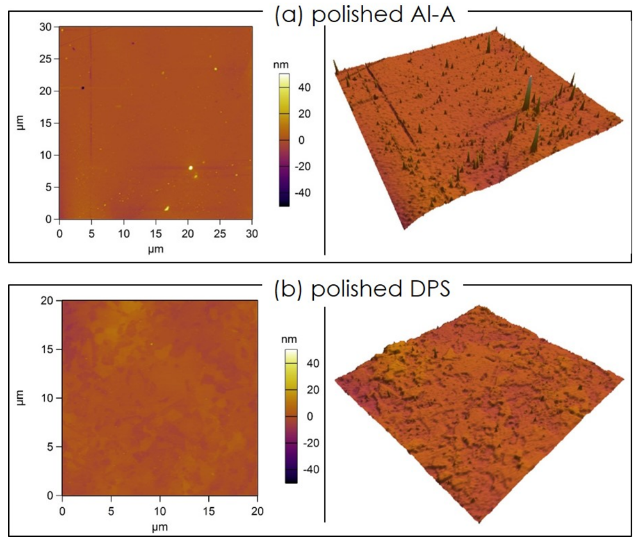

Figure 13. AFM images (2D and 3D) of polished metal samples: (a) Al-A and (b) DPS.

Table 8. Roughness Features of Metal Substrates Obtained from AFM Images and Radius of Asperity (r_2)

	surface characteristics		
metal sample	rms_2 (nm)	λ_2 (nm)	r_2 (μm)
Al-A (I)	1.18	706	7.28
DPS (I)	2.29	595	2.67
Al-A (II)	1.49	564	3.68
DPS (II)	1.75	480	2.27

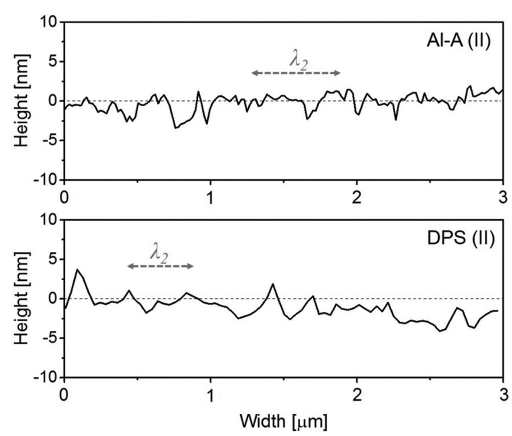

Figure 14. Roughness profiles (AFM section graphs) of polished metal samples.

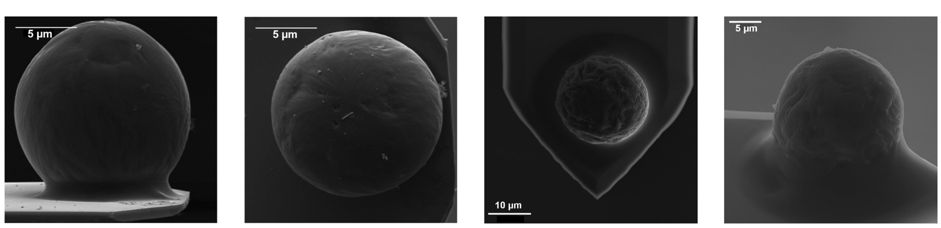

(a) (b) (c) (d)

Figure 12. SEM images of a (a and b) PA6 and (c and d) PE microsphere coated with a 5−10 nm carbon layer attached to a cantilever. SEM images were recorded at ZELMI, TU Berlin

DOI: 10.1021/acsami.5b01949
ACS Appl. Mater. Interfaces 2015, 7, 16247−16256

6.2. Methods. *6.2.1. AFM Force Measurements.* Force−distance curves were collected via an atomic force microscope (MFP3D, Asylum Research, CA, USA). Measurements were conducted in a dry nitrogen atmosphere at a constant temperature of 30 °C using a Poly Heater^{TM} cell (Asylum Research, Santa Barbara, CA) that can be fully sealed with a membrane. Prior to measurements, substrate and microsphere were immersed in pure ethanol for some minutes. The metal substrate was dried in a nitrogen stream before being placed in the cell. Before starting the experiment, we heated the cell, including the substrate and the colloidal probe, was heated to 60 °C for about 10 min under constant nitrogen flow in order to remove residual solvent. The humidity was kept under RH 5% throughout the whole measurement by flushing dry nitrogen through the cell. The flow was stopped when force−distance curves were recorded. A low humidity is necessary to exclude capillary forces.

Approaching and retracting force profiles were recorded at a velocity of 500 nm/s and a constant load of 1 or 2 μN, respectively. Statistical data evaluation is needed for a proper interpretation of the adhesion forces. Force maps including 100 single force−distance curves obtained over an area of 90 × 90 μm were recorded. At least five different locations of the sample were mapped. The procedure resulted in ≥500 single displacement−deflection curves for each probe−surface (polymer−metal) pair distributed over an area of approximately 0.04 mm^2. Measurements were repeated several times over a longer time period using at least two to three different microspheres. For analysis, a straight line is fitted to the noncontact region of the force−separation curves in order to account for possible drifts. The adhesion force is obtained from the minimum of the data of the retraction curve (see Figure 2). An adhesion histogram was generated from the results, and mean and standard deviation were calculated by fitting a Gaussian distribution to the histogram. As a control experiment, interaction forces between the polymeric probe and a silica wafer were measured regularly to validate the experimental setup and the state of the colloidal probe. Silica wafers exhibit a low surface roughness and stable surface composition. Force measurements using silica wafers as a substrate were proven to be reproducible with constant force values for a given polymer.

6.2.2. Contact Angle (CA) Measurements. For macroscopic studies of the adhesion properties CA measurements were performed using the sessile drop method. The work of adhesion per area W_{ad} between two materials, denoted 1 and 2, is given by the Dupré equation:[52]

$$W_{ad} = \gamma_1 + \gamma_2 - \gamma_{12} \tag{12}$$

where γ_1 and γ_2 are the surface free energies of the two solid materials, and γ_{12} is the interface free energy between them. Using the Fowkes approach[53] the surface energy is a sum of components with a dispersion γ^d and a polar part γ^p leading to the following relationship for the interfacial energy between materials 1 and 2:

$$\gamma_{12} = \gamma_1 + \gamma_2 - 2\sqrt{\gamma_1^d \gamma_2^d} - 2\sqrt{\gamma_1^p \gamma_2^p} \tag{13}$$

The surface energy of a solid (S) γ_S with a polar γ_S^p and dispersive γ_S^d part can only be experimentally determined against a series of probe liquids (L) with known γ_L^p and γ_L^d. For calculation of γ_S the Owens−Wendt−Rabel−Kaelble method (OWRK)[19,20] with the following equation is used:

$$\frac{(1 + \cos\theta)}{2}\frac{\gamma_L}{\sqrt{\gamma_L^d}} = \sqrt{\gamma_S^p}\frac{\sqrt{\gamma_L^p}}{\sqrt{\gamma_L^d}} + \sqrt{\gamma_S^d} \tag{14}$$

With at least two liquids, γ_S^d can be determined from the interception and γ_S^p from the slope of the OWRK plot.

Contact angles were measured with a Goniometer OCA20 (Dataphysics, Germany). Metal and polymer samples were cut into plates of 2 × 2 cm. The plates were cleaned with pure ethanol for 10 min in the ultrasonic bath (solvent degreasing) and subsequently dried with nitrogen. The clean samples were placed on a sample stage in a closed cell, which was filled by one-third with the respective test liquid in order to obtain a saturated atmosphere. Samples were equilibrated for around 30 min before a drop of the liquid is placed on the surface via a syringe. A 90 min video was recorded, and the contact angle was determined using the tangent fitting method. No large differences were observed between left and right contact angles; therefore, the average of both was taken as contact angle. Three to four different test liquids were used for each solid substrate. Several drops of each liquid were placed on different spots of the substrate and the equilibrium contact angle was averaged over all measurements. Measurements were repeated at least two times. The surface tension of the test liquids including their polar and dispersive parts are listed in Table 9.

Table 9. Total Surface Tension (γ_L) and Dispersive (γ_L^d) and polar (γ_L^p) Part for Various Test Liquids[a]

test liquid	total surface tension, γ_L (mN/m)	dispersive part, γ_L^d (mN/m)	polar part, γ_L^p (mN/m)
formamide	56.9	23.5	33.4
1-bromonaphthalene	44.4	44.4	0
diiodomethane	50.0	47.4	2.6
ethylene glycol	48.2	29.3	18.9
glycerol	63.3	20.2	43.1
water	72.8	21.8	51.0

[a]Values are taken from refs 54 and 55.

ASSOCIATED CONTENT

Supporting Information

Adhesion energy (E_{ad}) related to a microscopic work of adhesion per area. The Supporting Information is available free of charge on the ACS Publications website at DOI: 10.1021/acsami.5b01949.

AUTHOR INFORMATION

Corresponding Author

*Phone: +49 (30) 314 23476. Fax: +49 (30) 314 26602 E-mail: klitzing@chem.tu-berlin.de.

Notes

The authors declare no competing financial interest.

ACKNOWLEDGMENTS

The authors thank the Federal Ministry of Education and Research (BMBF) (WING Project Extra Light) and Technische Universität Berlin for the financial support.

REFERENCES

(1) Grujicic, M.; Sellappan, V.; Omar, M. A.; Seyr, N.; Obieglo, A.; Erdmann, M.; Holzleitner, J. An Overview of the Polymer-to-Metal Direct-Adhesion Hybrid Technologies for Load-Bearing Automotive Components. *J. Mater. Process. Technol.* **2008**, *197*, 363−373.

(2) Roesner, A.; Scheik, S.; Olowinsky, A.; Gillner, A.; Reisgen, U.; Schleser, M. Laser Assisted Joining of Plastic Metal Hybrids. *Phys. Procedia* **2011**, *12*, 370−377.

(3) Awaja, F.; Gilbert, M.; Kelly, G.; Fox, B.; Pigram, P. J. Adhesion of Polymers. *Prog. Polym. Sci.* **2009**, *34*, 948−968.

(4) Gasparin, A. L.; Wanke, C. H.; Nunes, R. C. R.; Tentardini, E. K.; Figueroa, C. A.; Baumvol, I. J. R.; Oliveira, R. V. B. An Experimental Method for the Determination of Metal-Polymer Adhesion. *Thin Solid Films* **2013**, *534*, 356−362.

(5) Ducker, W.; Senden, T.; Pashley, R. Direct Measurement of Colloidal Forces using an Atomic Force Microscope. *Nature* **1991**, *353*, 239−241.

(6) Kappl, M.; Butt, H. J. The Colloidal Probe Technique and its Application to Adhesion Force Measurements. *Part. Part. Syst. Charact.* **2002**, *19*, 129−143.

(7) Drelich, J.; Tormoen, G. W.; Beach, E. R. Determination of Solid Surface Tension from Particle-Substrate Pull-off Forces measured with the Atomic Force Microscope. *J. Colloid Interface Sci.* **2004**, *280*, 484−497.

(8) Drelich, J. Adhesion Forces measured Between Particles and Substrates with Nano-Roughness. *Miner. Metall. Process.* **2006**, *23*, 226−232.

(9) Beach, E. R.; Tormoen, G. W.; Drelich, J.; Han, R. Pull-Off Force Measurements Between Rough Surfaces by Atomic Force Microscopy. *J. Colloid Interface Sci.* **2002**, *247*, 84−99.

(10) Meine, K.; Kloss, K.; Schneider, T.; Spaltmann, D. The Influence of Surface Roughness on the Adhesion Force. *Surf. Interface Anal.* **2004**, *36*, 694−697.

(11) Kumar, A.; Staedler, T.; Jiang, X. Role of Relative Size of Asperities and Adhering Particles on the Adhesion Force. *J. Colloid Interface Sci.* **2013**, *409*, 211−218.

(12) Tormoen, G. W.; Drelich, J.; Nalaskowski, J. A Distribution of AFM Pull-Off Forces for Glass Microspheres on a Symmetrically Structured Rough Surface. *J. Adhes. Sci. Technol.* **2005**, *19*, 215−234.

(13) Yang, S.; Zhang, H.; Hsu, S. M. Correction of Random Surface Roughness on Colloidal Probes in Measuring Adhesions. *Langmuir* **2007**, *23*, 1195−1202.

(14) Liu, D. L.; Martin, J.; Burnham, N. A. Optimal Roughness for Minimal Adhesion. *Appl. Phys. Lett.* **2007**, *91*, 043107.

(15) Ramakrishna, S. N.; Clasohm, L. Y.; Rao, A.; Spencer, N. D. Controlling Adhesion Force by Means of Nanoscale Surface Roughness. *Langmuir* **2011**, *27*, 9972−9978.

(16) Schaefer, D. M.; Carpenter, M.; Gady, B.; Reifenberger, R.; Demejo, L. P.; Rimai, D. S. Surface-Roughness and its Influence on Particle Adhesion using Atomic-Force Techniques. *J. Adhes. Sci. Technol.* **1995**, *9*, 1049−1062.

(17) Gotzinger, M.; Peukert, W. Particle Adhesion Force Distributions on Rough Surfaces. *Langmuir* **2004**, *20*, 5298−5303.

(18) Chai, Z.; Liu, Y.; Lu, X.; He, D. Reducing Adhesion Force by Means of Atomic Layer Deposition of ZnO Films with Nanoscale Surface Roughness. *ACS Appl. Mater. Interfaces* **2014**, *6*, 3325−3330.

(19) Owens, D. K.; Wendt, R. C. Estimation of Surface Free Energy of Polymers. *J. Appl. Polym. Sci.* **1969**, *13*, 1741−1747.

(20) Kaelble, D. H. Dispersion-polar Surface Tension Properties of Organic Solids. *J. Adhes.* **1970**, *2*, 66−81.

(21) Cappella, B.; Dietler, G. Force-Distance Curves by Atomic Force Microscopy. *Surf. Sci. Rep.* **1999**, *34*, 1−104.

(22) Sarid, D., Ed. *Scanning Force Microscopy*; Oxford University Press: Cambridge, 1991.

(23) Wiesendanger, R., Ed. *Scanning Probe Microscopy and Spectroscopy: Methods and Applications*; Oxford University Press: Cambridge, 1994.

(24) Butt, H.; Cappella, B.; Kappl, M. Force Measurements with the Atomic Force Microscope: Technique, Interpretation and Applications. *Surf. Sci. Rep.* **2005**, *59*, 1−152.

(25) Hamaker, H. C. London-van der Waals Attraction Between Spherical Particles. *Physica* **1937**, *4*, 1058−1072.

(26) Johnson, K. L.; Kendall, K.; Roberts, A. D. Surface Energy and Contact of Elastic Solids. *Proc. R. Soc. London, Ser. A* **1971**, *324*, 301−313.

(27) Derjaguin, B.; Muller, V. M.; Toporov, Y. P. Effect of Contact Deformations on Adhesion of Particles. *J. Colloid Interface Sci.* **1975**, *53*, 314−326.

(28) Hertz, H. *Miscellaneous Papers*; Macmillan: London, 1896.

(29) Maugis, D., Ed. *Contact, Adhesion and Rupture of Elastic Solids*; Springer: Berlin, 2000.

(30) Schwarz, U. D. A. Generalized Analytical Model for the Elastic Deformation of an Adhesive Contact Between a Sphere and a Flat Surface. *J. Colloid Interface Sci.* **2003**, *261*, 99−106.

(31) Maugis, D. Adhesion of Spheres - the JKR-DMT Transition Using a Dugdale Model. *J. Colloid Interface Sci.* **1992**, *150*, 243−269.

(32) Rumpf, H. *Particle Technology*; Chapman and Hall: London, 1990.

(33) Rabinovich, Y. I.; Adler, J. J.; Ata, A.; Singh, R. K.; Moudgil, B. M. Adhesion Between Nanoscale Rough Surfaces - I. Role of Asperity Geometry. *J. Colloid Interface Sci.* **2000**, *232*, 10−16.

(34) Rabinovich, Y. I.; Adler, J. J.; Ata, A.; Singh, R. K.; Moudgil, B. M. Adhesion Between Nanoscale Rough Surfaces - II. Measurement and Comparison with Theory. *J. Colloid Interface Sci.* **2000**, *232*, 17−24.

(35) Laitinen, O.; Bauer, K.; Niinimaki, J.; Peuker, U. A. Validity of the Rumpf and the Rabinovich Adhesion Force Models for Alumina Substrates with Nanoscale Roughness. *Powder Technol.* **2013**, *246*, 545−552.

(36) Rudawska, A.; Jacniacka, E. Analysis for determining surface free energy uncertainty by the Owen-Wendt method. *Int. J. Adhes. Adhes.* **2009**, *29*, 451−457.

(37) Mantel, M.; Wightman, J. P. Influence of the Surface-chemistry on the Wettability of Stainless-Steel. *Surf. Interface Anal.* **1994**, *21*, 595−605.

(38) Fort, T. In *Contact Angle, Wettability, and Adhesion*; Fowkes, F., Ed.; American Chemical Society: Washington, D.C., 1964; Chapter 21.

(39) Fowkes, F. M. Attractive Forces At Interfaces. *Ind. Eng. Chem.* **1964**, *56*, 40−52.

(40) Kaftan, O.; Tumbiolo, S.; Dubreuil, F.; Auzely-Velty, R.; Fery, A.; Papastavrou, G. Probing Multivalent Host-Guest Interactions between Modified Polymer Layers by Direct Force Measurement. *J. Phys. Chem. B* **2011**, *115*, 7726−7735.

(41) Weder, G.; Voros, J.; Giazzon, M.; Matthey, N.; Heinzelmann, H.; Liley, M. Measuring cell adhesion forces during the cell cycle by force spectroscopy. *Biointerphases* **2009**, *4*, 27−34.

(42) Kirwan, L. J.; Maroni, P.; Behrens, S. H.; Papastavrou, G.; Borkovec, M. Interaction and Structure of Surfaces Coated by Poly(vinyl amines) of Different Line Charge Densities. *J. Phys. Chem. B* **2008**, *112*, 14609−14619.

(43) Pericet-Camara, R.; Papastavrou, G.; Behrens, S. H.; Helm, C. A.; Borkovec, M. Interaction forces and molecular adhesion between pre-adsorbed poly(ethylene imine) layers. *J. Colloid Interface Sci.* **2006**, *296*, 496−506.

(44) Thomas, R. C.; Houston, J. E.; Crooks, R. M.; Kim, T.; Michalske, T. A. Probing Adhesion Forces At the Molecular Scale. *J. Am. Chem. Soc.* **1995**, *117*, 3830−3834.

(45) Israelachivili, J. *Intermolecular and Surface Forces*, 2nd ed.; Academic Press: London, 1995.

(46) Maugis, D.; Pollock, H. M. Surface Forces Deformation and Adherence at Metal Microcontacts. *Acta Metall.* **1984**, *32*, 1323−1334.

(47) Zhou, H. B.; Gotzinger, M.; Peukert, W. The Influence of Particle Charge and Roughness on Particle-Substrate Adhesion. *Powder Technol.* **2003**, *135*, 82−91.

(48) Thio, B. J. R.; Meredith, J. C. Measurement of Polyamide and Polystyrene Adhesion with Coated-Tip Atomic Force Microscopy. *J. Colloid Interface Sci.* **2007**, *314*, 52−62.

(49) Neumann, A. W.; Omenyi, S.; Oss, C. Negative Hamaker Coefficients. 1. Particle Engulfment or Rejection at Solidification Fronts. *Colloid Polym. Sci.* **1979**, *257*, 413−419.

(50) Mott, P. H.; Roland, C. M. Limits to Poisson's Ratio in Isotropic Materials. *Phys. Rev. B: Condens. Matter Mater. Phys.* **2009**, *80*, 132104.

(51) Hutter, J.; Bechhoefer, J. Calibration of Atomic-force Microscope Tips. *Rev. Sci. Instrum.* **1993**, *64*, 1868−1873.

(52) Dupre, A. *Theorie mecanique de la chaleur*; Gauthier-Villars: Paris, 1869.

(53) Fowkes, F. M. Additivity of Intermolecular Forces at Interfaces. 1. Determination of Contribution to Surface and Interfacial Tensions of Dispersion Forces in Various Liquids. *J. Phys. Chem.* **1963**, *67*, 2538−2541.

(54) Busscher, H. J.; Vanpelt, A. W. J.; Deboer, P.; Dejong, H. P.; Arends, J. The Effect of Surface Roughening of Polymers on Measured Contact Angles of Liquids. *Colloids Surf.* **1984**, *9*, 319−331.

(55) Janczuk, B.; Bialopiotrowicz, T. Surface Free-energy Components of Liquids and Low-energy Solids and Contact Angles. *J. Colloid Interface Sci.* **1989**, *127*, 189−204.

DOI: 10.1021/acsami.5b01949
ACS Appl. Mater. Interfaces 2015, 7, 16247−16256